Journal of Molecular Modeling (2018) 24:344
https://doi.org/10.1007/s00894-018-3875-5

ORIGINAL PAPER

First report of a planar and a quasi-planar Al_{13}^+ cluster having localized antiaromatic deltas within an aromatic sea: NICS, ELF, AIM, and AdNDP bonding analysis

Surajit Guin[1] · Sourav Ranjan Ghosh[1,2] · Atish Dipankar Jana[1]

Received: 18 June 2018 / Accepted: 5 November 2018

Abstract
A perfectly planar Al_{13}^+ cluster (CI) and a quasi-planar Al_{13}^+ cluster (CII) have been found for the first time. Both clusters have a triangular core surrounded by a set of ten Al atoms in the form of a ring. These cationic clusters have substantial aromatic character. The planar CI cluster has local antiaromatic patches within global aromatic sea. It is doubly aromatic having both σ and π aromatic character. The quasi-planar CII cluster is also aromatic but it has more σ-delocalization.

Keywords Planar/quasi-planar aluminium cluster · NICS study · ELF analysis · AIM and AdNDP analysis · Aromaticity and antiaromaticity

Introduction

Neutral, anionic, as well as cationic aluminium clusters have drawn considerable attention of the scientific community in recent times [1–5]. These clusters have various important applications, such as catalyst [6], solid propellant for rocket [7], splitting of water [8], hydrogen storage [9], iodine absorption [10], magnetism [11], etc. Aluminium forms various stable clusters with sizes in the nanometer dimension having various shapes and geometries [12]. It has generally been seen that properties of clusters systematically vary with cluster size [13, 14]. At certain nuclearity n (n is the number of atoms in the cluster), clusters gain additional stability compared to adjacent clusters (n-1) and (n + 1). These more stable clusters are called magic clusters. Computations and experiment have revealed that only small Al clusters (n = 1–5) have planar geometry [12], but large Al_n [n = 6–65] clusters assume three-dimensional polyhedral structure [13–15].

For the first time, we report here a perfectly planar Al_{13}^+ cluster (CI) and a quasi-planar Al_{13}^+ cluster (CII), both having a triangular core surrounded by a set of ten aluminum atoms in the form of a ring (Fig. 1). Generally, as the number of atoms in a cluster increases, it tends to assume a three-dimensional geometry rather than a planar structure due to instability. Many of the previous studies involving Al clusters were aimed at determining the nuclearity [n] of the clusters at which the shape changes from the planar to the three-dimensional geometry [1–3]. These studies have revealed that for Al clusters, the transition from planar to three-dimensional geometry occurs when n changes from five to six. Thus, the planar (CI) and quasi-planar (CII) Al_{13}^+ clusters are by itself interesting findings and in the present paper we also report an in-depth study of the electronic structure of these clusters through quantum chemical computations. Unusual stability of many of the chemical systems has been attributed to electron delocalization, which renders aromatic character to them [16–18]. NICS parameter is a reliable indicator of aromaticity for planar systems and has been extensively used to establish the aromatic nature of planar chemical systems [19–22]. NICS(0) and NICS(1) are widely used in literature to unravel aromatic/antiaromatic character of planar chemical systems. NICS(1) is considered to be a better indicator of aromaticity

Surajit Guin and Sourav Ranjan Ghosh contributed equally to this work.

Electronic supplementary material The online version of this article (https://doi.org/10.1007/s00894-018-3875-5) contains supplementary material, which is available to authorized users.

✉ Atish Dipankar Jana
atishdipankarjana@yahoo.in; atish@behalacollege.in

[1] Department of Physics, Behala College, Parnasree, Kolkata 700060, India

[2] Department of Physics, Heritage Institute of Technology, Kolkata 700107, India

Published online: 24 November 2018

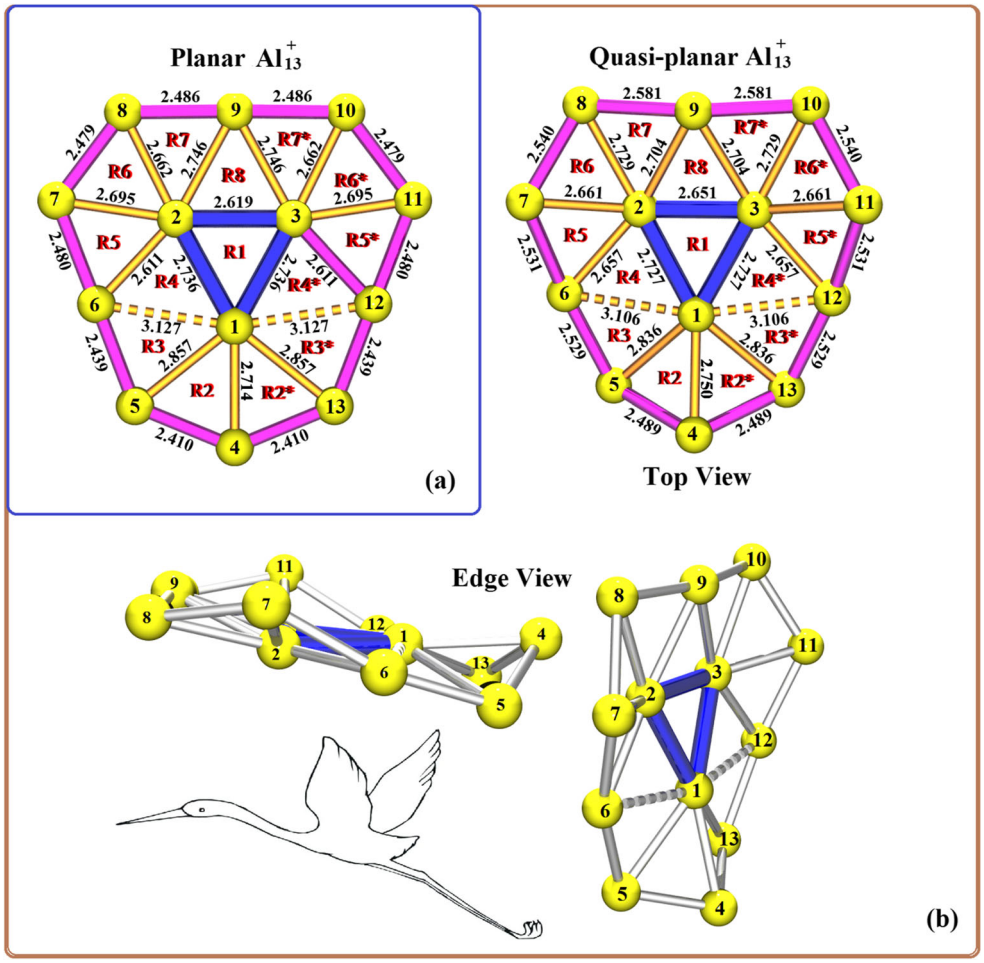

Fig. 1 Optimized geometry of **a** planar Al_{13}^+ clusters (CI) and **b** quasi-planar Al_{13}^+ clusters (CII). Bond distances labeled on the pictures are in Å units

as it is free from the contamination of the in-plane atoms, which is generally associated with NICS(0). We have computed both NICS(0) and NICS(1) over planes parallel to the cluster surface of planar CII in order to determine the spatial distribution of the NICS values. This study reveals a unique aromatic character of the planar Al_{13}^+ cluster—it is a cluster with three local antiaromatic deltas immersed within a global aromatic sea. For the quasi-planar CII cluster, we have computed NICS at the centers of the triangular subspaces within the cluster. NICS studies have been supplemented with the adaptive natural density partitioning (AdNDP) analysis [23–25], which provides a closer view of the nature of chemical bonding. AdNDP analysis reveals that both σ and π electron delocalization play an important role in the aromatic/antiaromatic character of planar Al_{13}^+ cluster. Electron localization function (ELF) [26] is also another tool for exploring the localized and delocalized character of electrons in an atomic cluster. Both ELF_π and ELF_σ show substantial delocalization of the π and σ electron cloud for the planar Al_{13}^+ cluster. Bader's atom in molecule (AIM) theory provides a topological view of a molecular or atomic cluster system [27]. In the topological analysis, molecular space is partitioned and assigned to individual atoms constituting the molecule. We have carried out AIM analysis for both the Al_{13}^+ cluster and this provides important information regarding the critical points and critical paths of both the clusters.

Computational methodology

DFT methodology has been employed to compute the geometry of both the Al_{13}^+ clusters. Computations have been carried out with the 6–311 + G(d) basis set [28] with B3LYP hybrid density functional. Here, a diffuse function has been introduced as the cluster under study is a cationic one. Polarization function has been used to study the effect of overlapping of orbitals. The harmonic frequency analysis of the computed structures reveal that the planar Al_{13}^+ cluster (CI) has three imaginary frequencies but the quasi-planar Al_{13}^+ cluster (CII) has zero imaginary frequency, indicating that CII is a true minimum structure. All optimizations and harmonic frequency analysis have been carried out with the help of GAUSSIAN-03 package [29]. AdNDP calculation has been carried out with the natural bond orbitals (NBO) computed at the B3LYP/6–311 + G(d) level by GAUSSIAN-03

package and subsequent analysis of AdNDP orbitals by employing the Multiwfn-3.5 program suit [30]. ELF and AIM analysis have also been carried out with the Multiwfn-3.5 program suit. Graphics for canonical orbitals and electro static potential (ESP) were generated using Molekel [31] and Chemissian package [32].

Results

Optimized structure of planar Al_{13}^+ cluster (CI)

Optimized geometry of the planar Al_{13}^+ cluster (CI) with atom numbering scheme has been depicted in Fig. 1a. The cluster has a planar geometry and a leaf-like shape. Its upper end is broad, but the dimension gradually shrinks towards the lower end. The cluster has a triangular core that is encircled by a set of ten aluminium atoms forming a peripheral ring. The core is an isosceles triangle formed by three aluminium atoms Al(1), Al(2), and Al(3). Al(1)-Al(2) and Al(1)-Al(3) distances are equal (2.736 Å), whereas Al(2)-Al(3) distance is nearly 0.117 Å smaller (2.619 Å) (Table S1). On the other hand, the inter atomic distances among the ten peripheral Al atoms (Al(4) to Al(13)) fall within the range 2.411 Å to 2.486 Å. As can be observed from the data in Table S1, Al–Al bond distances in the cluster distinctly fall into two categories (i) the core, for which the intra core Al-Al bond distances are relatively higher (2.619 Å to 2.736 Å) and (ii) the periphery, for which intra periphery Al-Al bond distances are in a distinctly lower range (2.410 Å to 2.486 Å). The peripheral ring Al atoms are connected to the three core Al atoms in such a way that each pair of Al atoms at the periphery form a triangle with the one of the three core Al atoms. Whereas Al(2) and Al(3) each form four core-periphery bonds, Al(1) form five core periphery bonds. Thus, in total, Al(1) has seven bonds, but Al(2) and Al(3) each has six bonds with their neighbors. Bond distances of three central Al atoms with the peripheral Al atoms fall in the range 2.611 Å to 3.127 Å. Al(1)-Al(6) and Al(1)-Al(12) bond distances (3.127 Å) are relatively higher compared to other Al(1) bonds. There is also a systematic increase in the intra peripheral Al-Al distances. At the lower end, it is shortest (2.410 Å), which systematically increases to 2.486 Å at the upper end of the cluster. The cluster has a bilateral symmetry, the symmetry line passes through Al(4) at lower tip, Al(1) at the core and Al(9) at the middle of the top edge. These three atoms lie almost along a line.

Optimized structure of quasi-planar Al_{13}^+ cluster (CII)

The energy of the optimized CII cluster is − 3151.694418 Hartree. For a comparison, the energy of the CI cluster at the same level of theory is − 3151.682891 Hartree. Overall core-periphery arrangement of CII cluster (Fig. 1b) is identical to that of CI cluster—an isosceles triangular core is surrounded by a set of ten peripheral Al atoms. This cluster also possesses the same bilateral symmetry as that of CI. The symmetry line passes through the same set of three atoms (Al(4), Al(1), and Al(9)). The triangular core of CII cluster is more compact compared to CI cluster. In the core, Al(1)-Al(2) and Al(1)-Al(3) distances are equal (2.727 Å), whereas Al(2)-Al(3) distance is shorter (2.619 Å) (Table S1). Both the longer bonds as well as the shorter bond of the isosceles triangular core of CII cluster is small compared to that of the CI cluster. On the other hand, the Al-Al distances on the periphery of the CII cluster is larger compared to the corresponding Al-Al distances in the CI cluster. Inter-atomic distances among the ten peripheral Al atoms (Al(4) to Al(13)) for CII cluster fall within the range 2.489 Å to 2.581 Å. A systematic increase of bond distances from the bottom to the top of the cluster along the periphery is evident in the successive increase of the bond lengths along the periphery (Al(4)-Al(5) = 2.489 Å, Al(5)-Al(6) = 2.529 Å, Al(6)-Al(7) = 2.531 Å, Al(7)-Al(8) = 2.540 Å and Al(8)-Al(9) = 2.581 Å). This nature is identical to that found in CI.

The main structural difference between CI and CII cluster is the non-planarity of the later. Whereas all atoms in the CI cluster lie in the same plane, for the CII cluster, atoms lying on the periphery are situated above and below the mean plane passing through the three central atoms (Al(1), Al(2), and Al(3)) constituting the core of the cluster. Al(9) and Al(4) atoms lying on the bilateral symmetry line are, respectively, 0.858 Å and 0.239 Å above this mean plane. Two symmetry-related atoms Al(8) and Al(10) are 0.603 Å above the mean plane. Al(7) and Al(11) are most deviated from this mean plane by an amount 1.032 Å. Al(6) and Al(12) are slightly down of this mean plane (0.162 Å). Al(5) and Al(13) are deviated maximally downward from the mean plane by an amount 0.842 Å. The planes of two symmetry-related rings R4 and R4* that share a common edge with central isosceles triangular ring R1, deviate downward by 3.21°. Ring R8 at the top of the cluster, which shares the shorter edge of R1, deviated upward by 21.26°. The configuration of the cluster can be compared with that of a flying bird with its wings up. The head part of CII is constituted by five conjoined triangles (R6, R7, R8, R9, and R10). The upward wings are constituted by two conjoined triangles R2, R3 and R2*, R3*, where the peripheral atoms Al(6) and Al(12) deviate maximally downwards. Al(4), which is above the mean plane, share common edge of two adjacent triangles R2, R2* constituting the tail of the cluster.

Like CI, in CII also Al–Al bond distances fall into (i) core and (ii) periphery category. Core Al-Al bonds fall in a high range (2.615 Å to 2.727 Å) than the peripheral Al-Al bonds (2.489 Å to 2.581 Å). Similar core-periphery bonding pattern is also present in this cluster.

Electrostatic potential surface, Mulliken charge distribution, and dipole moment

Electrostatic potential (ESP) surfaces and Mulliken charge distributions for both the clusters have been pictorially depicted in Fig. 2. Figure 2a, b depict the ESP surfaces of planar and quasi-planar clusters CI and CII, respectively. For both the clusters, the electrostatic potential surfaces clearly show that core and periphery of the cluster is distinctly demarcated. The core has a high negative charge concentration. It is surrounded by gradually increasing positive charge concentrations.

It can be seen from Fig. 2a that the deep-red region corresponding to the highest negative charge concentration is located over two atoms Al(2) and Al(3) at the core of the cluster (see also Fig. 1a). Al(1) also bears a negative charge. This is indicated by yellow color ESP surface at the location of this atom. That the positive charges are located around the periphery of the cluster is evident in the presence of blue color ESP surfaces there. The deepest blue spots are located over Al(5) and symmetry related Al(13). Both the top left and top right corners of the cluster are also having blue ESP iso-surfaces. Al(7), Al(8), and symmetry related Al(10), Al(11) are located at the top left corner and top right corner, respectively.

For the quasi-planar CII cluster, the deepest red spot corresponding to the highest negative charge occurs on Al(1). It can be noted that the negative charge concentration on Al(1) in CII is higher than that of CI. Al(2) and Al(3) are also negative charge centers but have lesser charge density compared to Al(1). The deepest blue regions over the ESP surface corresponding to positive charge concentrations for this cluster appear at the top left and top right corners of the cluster.

The distribution of Mulliken charges over the atoms of the clusters CI and CII have been depicted in Fig. 2c, d, respectively. The nature of Mulliken charge distribution nicely correlates with the nature of the ESP surface. The charge distribution has an inherent bilateral symmetry. The core of both the clusters is the seat of negative charges and the peripheral ring is the seat of positive charges. Mulliken charges for individual atoms for both the clusters have been collected in Table S2.

In CI cluster Al(2) and Al(3) bear equal amount of highest negative charge. The negative charge on Al(1) is nearly one-third of that borne by Al(2) or Al(3) (Table S2). On the other hand, the highest negative charge for CII occur on Al(1) instead of Al(2) or Al(3). The magnitude of negative charge concentration on Al(1) in CII is even higher than the highest negative charge on Al(2) and Al(3) of CI. The amount of negative charge on Al(2) and Al(3) of CII is little small compared to that of CI. For CI, the highest positive charge is concentrated around the lower end of the cluster on Al(5) and Al(13). Al(9) at the middle of the top edge of the cluster is nearly neutral bearing a very little negative charge.

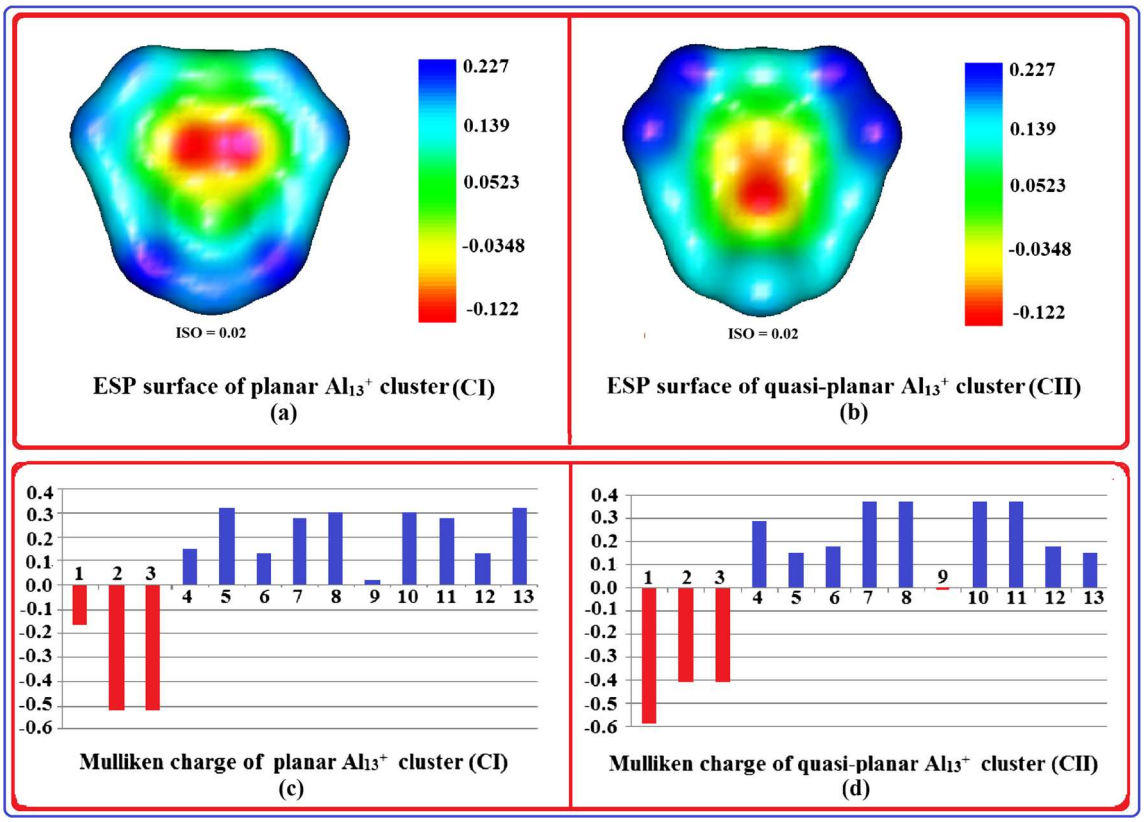

Fig. 2 Electrostatic potential map and Mulliken charge distribution of Al_{13}^{+} clusters

Concentration of positive charge on the left edge of the cluster has a dip on Al(6). Positive charge concentration on Al(7) and Al(8) is quite high. For CII, the highest positive charge of nearly equal magnitude is located on Al(7), Al(8) and their symmetry related Al(10), Al(11). The positive charge concentration on Al(5) in this cluster is somewhat smaller than that of Al(5) in CI. The positive charge density of Al(6) of CII is a little higher than that of CI. Whereas in CI the charge density on Al(9) has a small positive value, in CII it has become slightly negative.

From the comparison of charge distribution of CI and CII, it can be concluded that although the macro nature of the charge distribution is the same in both the clusters, the micro nature is quite different. In both the clusters, the core is the seat of negative charge and the periphery is the seat of positive charge, but there is more negative charge at the core of CII than that of CI. This charge transfer makes the periphery of CII overall more positive compared to that of CI.

The nature of dipole moment of both the clusters is in accordance with the charge distribution in respective clusters. Dipole moments of both the clusters are directed along the bilateral symmetry axis. The directions of the dipole moments are opposite to each other—in CI it is directed from top to bottom along the symmetry line, but in CII it is directed from bottom to top. The magnitude of dipole moment in CII is more (1.2198 Debye) compared to that of CI (0.9689 Debye) (Table 1). This clearly indicates that there is more charge separation in CII.

Canonical molecular orbitals

HOMO, LUMO, and relevant delocalized orbitals of CI and CII clusters have been shown in Fig. 3a, b, respectively. Frontier orbitals HOMO and LUMO are directly related to the reactivity of a cluster. The HOMO-LUMO gap for the planar CI cluster is 1.557 eV and that of CII is 1.373 eV. HOMO for CI is substantially delocalized and is having mostly π-character. On the other hand, LUMO is less delocalized and having mostly σ-electron contribution. For the CII cluster, HOMO is located over the periphery of the cluster. It has mostly sigma character except at the top edge, where a mixed π-σ character is visible. LUMO for CII is banded in nature and is having π-character. HOMO-1 and HOMO-2, in the CI cluster, have substantial delocalization along the periphery of the cluster. They have mostly π-character. HOMO-6 is completely delocalized over the whole surface of the cluster. Other orbitals also have a varying amount of delocalization (Fig. 3a).

For the CII cluster, HOMO-1 is also delocalized and having mostly π-electron contribution. HOMO-6 has π-character. It is delocalized over the upper-half of the cluster. Other orbitals also have a varying amount of delocalization (Fig. 3a).

Table 1 Dipole moments of Al_{13}^+ clusters

Dipole moment (Debye)	Al_{13}^+ (CI)	Al_{13}^+ (CII)
μ_x	− 0.0002	0.0001
μ_y	0.9689	− 1.1406
μ_z	0.0000	0.4325
$\lvert\mu\rvert$	0.9689	1.2198

NICS study

NICS(0) and NICS(1) surface plots characterizing the aromatic nature of the planar CI cluster are depicted in Fig. 4. As can be seen from these plots, bands of positive and negative NICS regions appear one by one from the top towards the bottom of the cluster. Whereas in the NICS(0) plot four bands in the sequence of positive, negative, positive and negative NICS(0) values appear, in the NICS(1) plot a Y-shaped central band of negative NICS(1) values is intertwined with three regions of positive NICS(1) values. Negative NICS values indicate aromatic regions and the positive NICS values indicate antiaromatic regions. Small absolute values of NICS (0 ppm – 5 ppm) indicate non-aromatic regions. It can be seen from Fig. 4 that in the NICS(0) plot the first band of aromatic region lies along the bonds connecting Al(7), Al(2), Al(3), and Al(11). The highest negative contour line passing over this region has a value of - 10 ppm. This line also passes though the central triangular core of the cluster consisting of Al(1), Al(2), and Al(3). It can be noticed that two bonds Al(1)-Al(2) and Al(1)-Al(3) are sandwiched between contour lines of - 10 ppm, which means at the middle of these bonds the NICS(0) values are still higher (~ − 15 ppm). The second aromatic band lies at the lower end of the cluster spanned over Al(4), Al(5), and Al(13) atoms. The - 15 ppm contour line touches the center of the two bonds Al(4)-Al(5) and Al(4)-Al(13). Among two antiaromatic bands in the NICS(0) plot, one is located at the upper end of the cluster and the other one is located just above three lower Al atoms Al(4), Al(5) and Al(13). There are three antiaromatic hot-spots (light blue regions in [Fig. 4a]) with NICS values +15 ppm.

In the NICS(1) surface plot, the regions of aromatic and antiaromatic ones are clearly distinguishable. A single Y-shaped aromatic band is located above the second row of Al atoms [Al(7), Al(2), Al(3), and Al(11)] and Al(1) and Al(4). The highest negative contour line (− 15 ppm) is located around the bonds Al(7)-Al(8) and Al(10)-Al(11) (Fig. 4b). Over most of the central triangular core, the NICS value is between - 5 ppm and - 6 ppm. Two antiaromatic regions are clearly located over the bonds Al(5)-Al(6) and Al(12)-Al(13). The highest positive NICS(1) contour line in these regions has a value of + 9 ppm. The region around Al(9) at the upper end of the cluster is also overlain by a region of antiaromaticity.

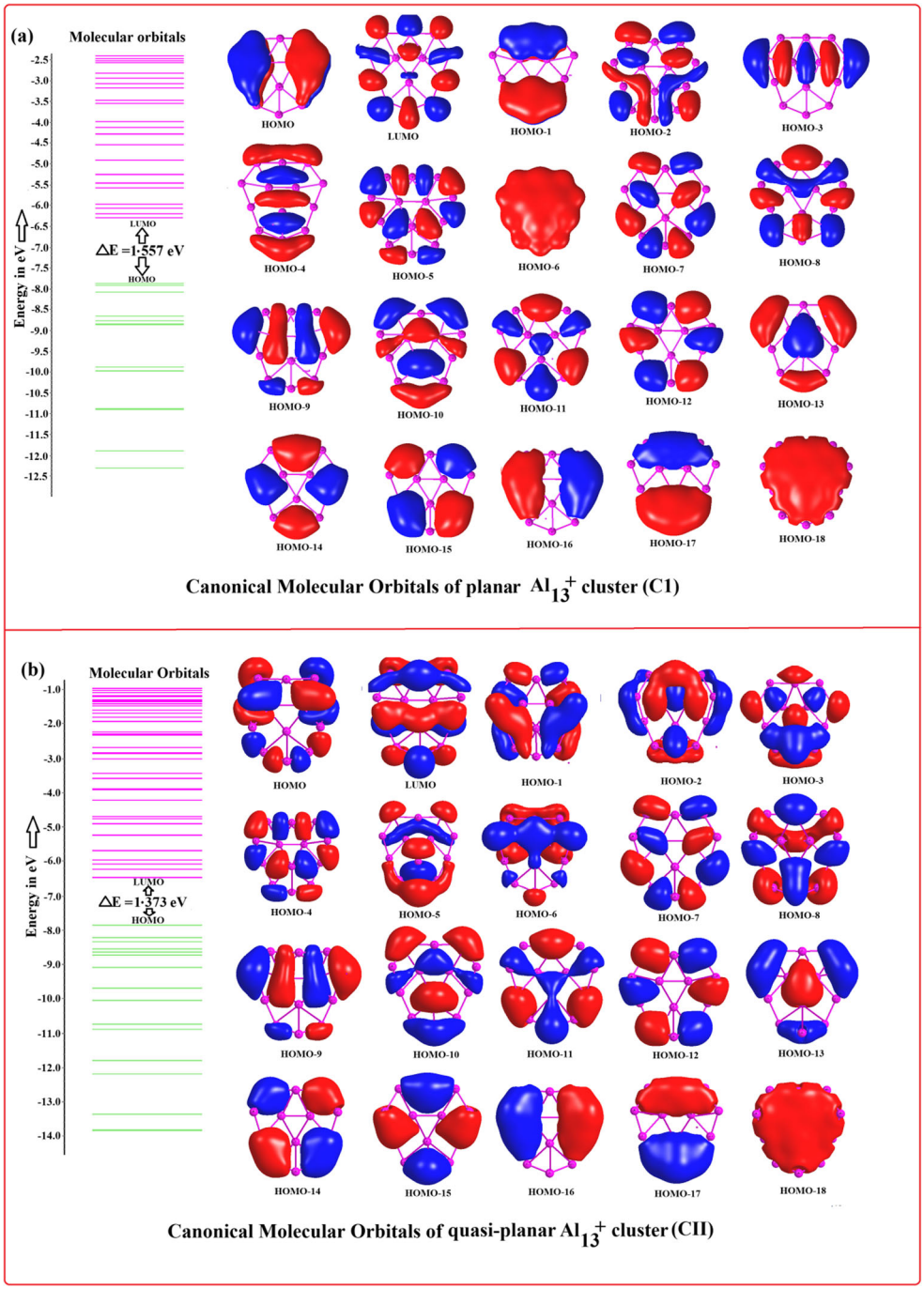

Fig. 3 Selected delocalized orbitals of **a** planar CI and **b** quasi-planar CII cluster

The observed variation of both NICS(0) and NICS(1) nicely correlates with the structural features of the cluster. It is expected that the bond lengths around the antiaromatic regions should be longer compared to that of the aromatic regions. From Fig. 1a, one can see that larger bond lengths (3.127 Å) for Al(1)-Al(6), Al(1)-Al(12) and (2.857 Å) for Al(1)-Al(5), Al(1)-Al(13) can be assigned to their proximity to antiaromatic regions shown in Fig. 4a. These bonds form the triangular subspaces R3 and R3*, which exactly coincides with the antiaromatic region on the NICS surface plot. Similar is the case for the second highest bond lengths (2.746 Å) in the cluster, which occurs for Al(9)-Al(2) and Al(9)-Al(3) bonds. The topmost antiaromatic hot-spot in the NICS(0) plot is sandwiched between these two bonds (Fig. 4a). On the other hand, the shortest bond lengths (2.410 Å) for Al(4)-Al(5) and Al(4)-Al(13) can be assigned to the superposition of the strongest aromatic band over these bonds. Similar correlation of shortening of bond length with the aromaticity can be observed for bonds Al(7)-Al(8) and Al(10)-Al(11), which are distinctly smaller (2.479 Å) compared to two adjacent

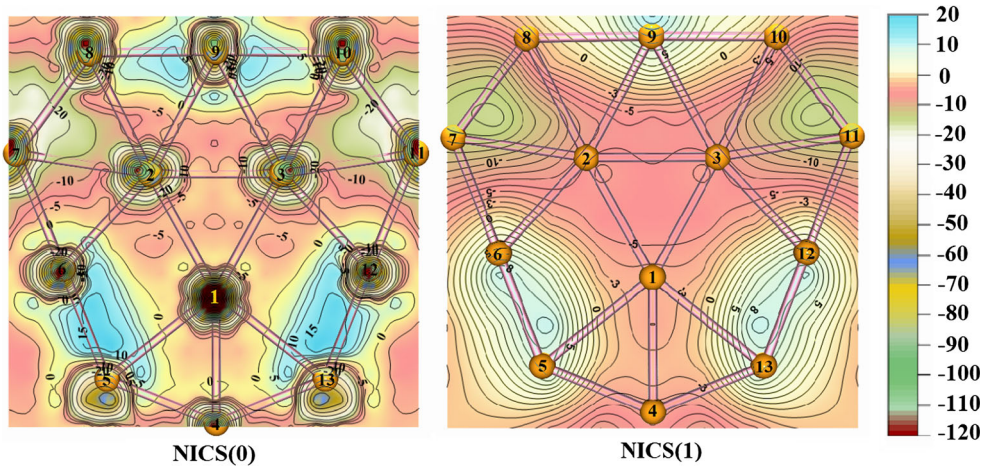

Fig. 4 **a** NICS(0) and **b** NICS(1) surface plot for the planar Al_{13}^{+} cluster (CI)

peripheral bonds on either side, 2.486 Å [for Al(8)-Al(9) and Al(10)-Al(11)] and 2.480 Å [for Al(6)-Al(7) and Al(11)-Al(12)]. Both NICS(0) and NICS(1) surface plots show the presence of quite a strong aromatic band over these bonds (− 10 ppm) in NICS(0) and - 15 ppm in NICS(1)). A comparison of NICS(0) and NICS(1) surface plot shows that overall the nature of distribution of aromatic and antiaromatic regions with height remains more or less same. The main difference between NICS(0) and NICS(1) surface plot is that whereas in NICS(0) the region around the bond Al(1)-Al(4) is non-aromatic (NICS(0) value is nearly 0 ppm)) at 1 Å above, this region shows negative NICS(1) values (− 3 ppm). This leads to the joining of the two separate aromatic bands of the NICS(0) plot into a single aromatic Y-shaped band. The relatively shorter Al(1)-Al(4) bond length (2.714 Å) can be assigned to this aromatic band.

An elaborate study on the variation of NICS with height (hereafter NICS(z)) has been performed for both CI and CII. CII being non planar NICS surface study was not carried out for this. NICS(z) have been calculated at the center of each of 14 triangular subspaces from -5 Å to +5 Å with respect to the mean plane of each triangle (Fig. 5). For both CI and CII, NICS(z) values remain negative for 12 of the 14 triangular subspaces. Only for the rings R3 and R3* the NICS(z) values are seen to be positive.

For the planar cluster CI, NICS(z) through the center of the ring R1 show two minima at z = ± 0.5 Å having same value − 6.18 ppm (Fig. 5a). For CII, the NICS(z) has been shown in Fig. 5b. NICS(z) in this case is not symmetric about z = 0 plane as the positive z space and negative z space are different due to non-planarity of the cluster. Highest negative NICS(z) value (− 5.05 ppm) occurs z = +0.5 Å (Table 2). In the negative direction, there is another deep (− 4.40 ppm) at z = − 1.0 Å. The negative value of NICS(z) gradually decreases with height and tends to zero values for both CI and CII.

NICS(z) at the center of ring R2 (and symmetry related ring R2*) also shows two minima with value, − 1.93 ppm for CI at z = ± 0.5 Å. For the CII cluster, the highest negative NICS(z) value of − 5.49 ppm occurs at z = − 1 Å. The variation is asymmetric as expected. As one advances towards the positive z direction from z = − 1 Å, NICS(z) becomes zero at z = 0 Å then becomes slightly positive (2.33 ppm) at z = + 0.5 Å and then gradually decreases to zero.

Variation of NICS with height at the center of rings R3 and R3* for both CI and CII show positive NICS(z) values indicating the antiaromatic nature of this triangular sub-region. The highest positive NICS value (+ 10.54 ppm) occurs for CI at height z = 0 Å. For CII cluster the highest positive NICS value (+ 7.68 ppm) occurs at z = 0 Å.

Variation of NICS with height at the center of R4 (and R4*) shows that the highest negative NICS value − 5.66 ppm for CI occurs at z = 0 Å. For the corresponding rings of CII, the highest negative NICS value is little higher (− 6.59 ppm), which occur at z = 1.0 Å.

For rings R5 and R5*, the highest negative NICS values (− 7.62 ppm for CI and − 13.59 ppm for CII) occur at heights z = ± 0.5 Å for CI and − 0.5 Å for CII. For rings R6 and R6*, highest negative NICS values (− 19.12 ppm for CI and − 18.03 ppm for CII) occur at z = 0 Å level. At the center of R7 and R7*, maximum gain in aromaticity occurs for CII. For these rings, the highest negative NICS value for CII cluster is − 9.62 ppm at a height of 0.5 Å, whereas for CI cluster highest negative NICS values of − 1.88 ppm occur at heights z = ± 1.0 Å. At the center of ring R8, there is also an increase of aromaticity for CII. The highest negative NICS value (− 10.45 ppm) occurs at z = − 0.5 Å for CII. For CI, this value is − 7.89 ppm at z = 0 Å level. For most of the rings, NICS(z) decreases to zero values beyond approximately 2.5 Å on either side of the ring planes. In Table 2, we have summarized the highest NICS values for the both the clusters at corresponding rings. It can be noted that the CII cluster gains aromaticity for

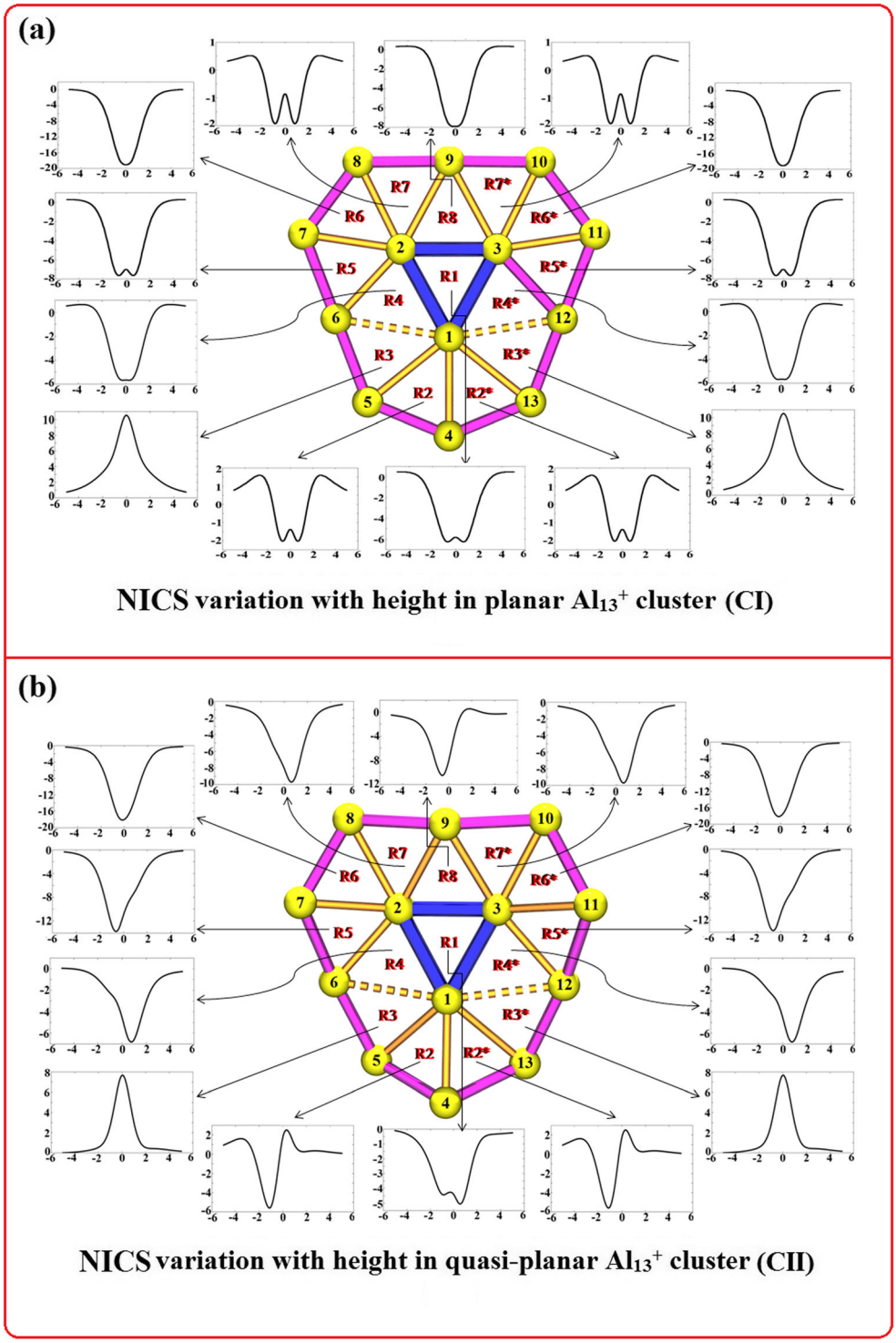

Fig. 5 Variation of NICS with height from the mean plane of triangular subspaces in CI and CII

most of the triangular sub-spaces by adopting a quasi-planar structure. At rings R1, R1* and R6, R6*, it slightly loses aromaticity (1.13 ppm and 1.10 ppm, respectively) but in all other rings it gains in aromaticity appreciably (Fig. 6) with a net gain of aromaticity of magnitude 41.37 ppm.

Electron localization function (ELF) analysis

Becke and Edgecombe first introduced electron localization function (ELF) [33], which was an extension of the work reported by Bader et al. [34]. For an electron at a point r, ELF is an inverse measure of the probability of a second

Table 2 Comparison of highest NICS(z) values at triangular sub-spaces of CI and CII cluster

Cluster	CI		CII		Gain/Loss of aromaticity of CII (ppm)
	Highest NICS(z) (ppm)	Height where maximum occur (Å)	Highest NICS(z) (ppm)	Height where maximum occur (Å)	
R1	− 6.18	± 0.5	− 5.05	+ 0.5	− 1.13
R2 and R2*	− 1.93	± 0.5	− 5.49	− 1.0	+ 3.56
R3 and R3*	+ 10.54	0.0	+ 7.68	0.0	+ 2.86
R4 and R4*	− 5.66	0.0	− 6.59	1.0	+ 0.93
R5 and R5*	− 7.62	± 0.5	− 13.59	− 0.5	+ 5.97
R6 and R6*	− 19.12	0.0	− 18.03	0.0	− 1.09
R7 and R7*	− 1.88	± 1.0	− 9.62	0.5	+ 7.74
R8	− 7.89	0.0	− 10.45	− 0.5	+ 2.56
Overall gain of aromaticity of CII cluster = (2*(3.56 + 2.86 + 0.93 + 5.97–1.09 + 7.74) + (2.56–1.13))ppm = 41.37 ppm					

electron having the same spin being in the immediate vicinity of the first electron. ELF is a dimensionless quantity and its value varies between zero and one. The closer the value of ELF is to one, the lower is the probability of the same-spin electron being near the electron at some position r and the higher is the level of localization of the electron at that point. Values of ELF close to one have been found to characterize localized pairs of opposite spin electrons, e.g., lone pairs and covalent bonds [35]. ELF recovers the Lewis picture of molecular bonding and provides graphical representations of molecular systems. ELF can be separately calculated for both π-electrons (called ELF_{π}) and for σ-electrons (called ELF_{σ}). As this decomposition can easily be done only for perfectly planar systems, we use here total ELF for comparing the aromatic nature of CI and CII clusters. The results of total ELF analysis have been depicted in Fig. 7.

Total electron localization function of the CI cluster (Fig. 7a) reveals that at an iso-value of 0.70, the ELF surface consists of five distinct islands spread over the periphery of the cluster. The smallest of these islands is localized in between Al(5), Al(6), and their symmetry-related counterparts Al(12), Al(13). An ELF iso-surface having a 'V' shape is delocalized at the lower tip of the cluster around Al(4). Tips of this iso-surface are located at the middle of the bonds Al(4)-Al(13) and Al(4)-Al(5). Two symmetry-related ELF zones having a 'ε' shape and highest spatial extension are located at the upper left and the upper right corner of the cluster around Al(7), Al(8) and Al(10), Al(11). Three tips of the left 'ε'-shaped iso-surface are located over the triangles R5, R6, and R7. An anchor-shaped ELF island is also present at the triangular core of the cluster.

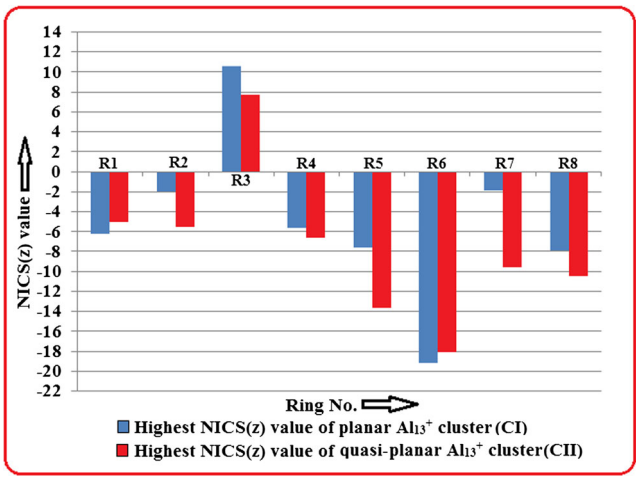

Fig. 6 Highest NICS(z) values at different ring centers of the CI and CII

These results are quite consistent with the results from the NICS analysis. In the NICS analysis, it has been seen that the antiaromatic region is localized over triangle R3 consisting of Al(1), Al(5), and Al(6). This region is also devoid of any ELF iso-surface. NICS analysis also revealed that the highest aromatic region of the cluster is at the top left corner and at the top right corner. The 'ε'-shaped ELF iso-surface is most prominent and continuous over these regions. The lower tip region of the cluster is also moderately aromatic. Here also ELF reveals a 'V'-shaped continuous iso-surface. At a higher iso-value of 0.72, this 'V'-shaped iso-surface first bifurcates. The 'ε'-shaped ELF iso-surface bifurcates into two fragments at an iso-value of 0.81. Completer bifurcation of these occurs at an iso-value of 0.87.

Total electron localization function for the quasi-planar CII cluster has been depicted in (Fig. 7b). The iso-surface plot at 0.70 shows only two distinct islands over the periphery of the cluster in comparison to five islands of CI. Except at the locations of Al(6) and Al(12), these two ELF islands completely fill the peripheral Al atoms. At the triangular core, there is also a continuous ELF iso-surface having better spatial coverage than that of CI. Thus, it can be concluded that in CII, electrons are more delocalized over the periphery as well as the core of

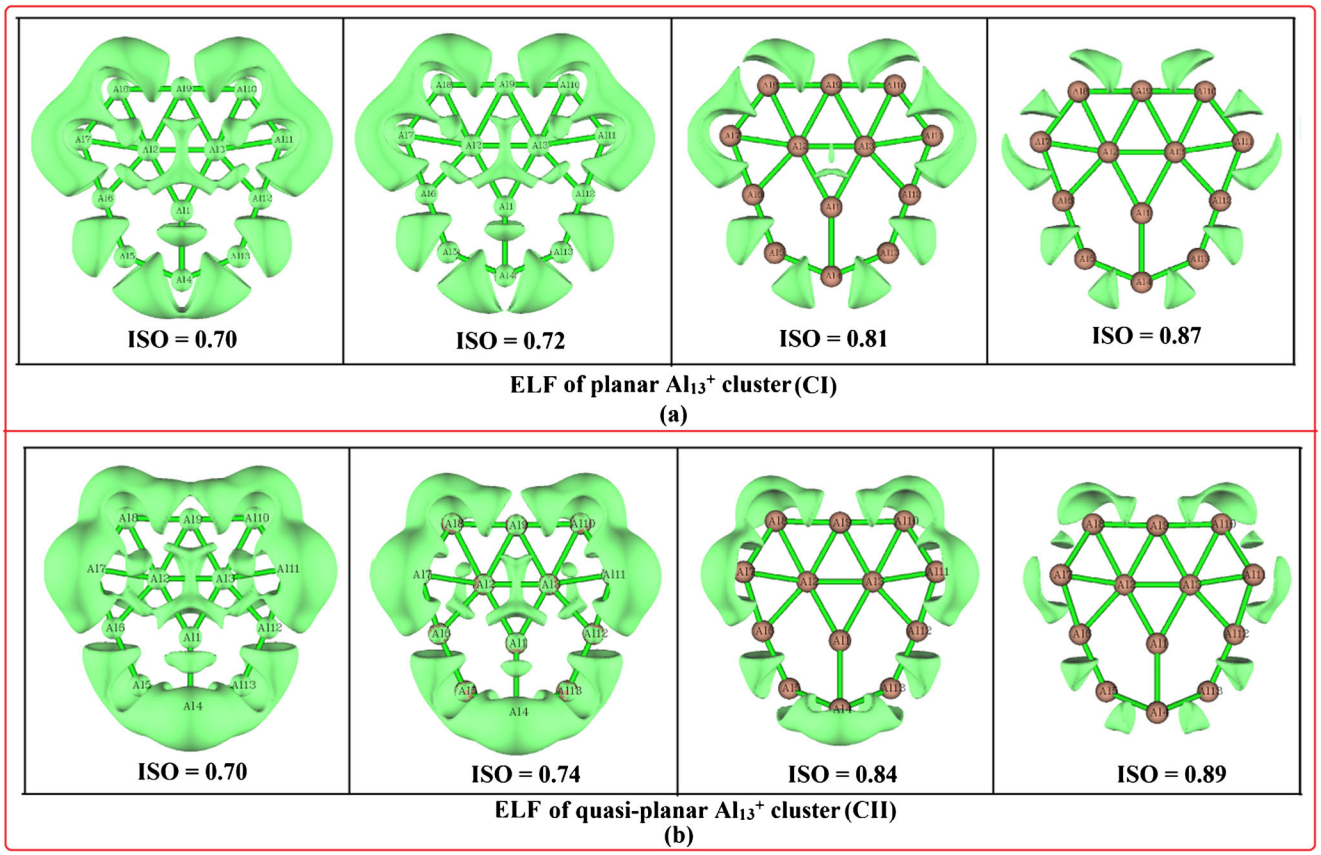

Fig. 7 Total ELF analysis of CI and CII cluster

the cluster. This correlates well with the NICS results, which show higher average global aromatic nature for CII compared to CI.

At an iso-value of 0.74, the upper ELF iso-surface over the periphery first bifurcates at the location of Al(9). The lower ELF iso-surface over the periphery bifurcates at an iso-value of 0.84 at the location of atoms Al(5) and Al(13). Complete bifurcation of ELF iso-surfaces occurs at an iso-value of 0.89.

For gaining further insight into the contribution of π and σ electrons to the electron delocalization and aromatic character of the planar CI cluster, we have carried out both ELF_{π} (Fig. S1) and ElF_{σ} (Fig. S2) analysis. For ELF_{π}, the iso-surface plot at 0.70 iso-value shows two distinct islands over the cluster. The lower island encloses four atoms Al(1), Al(4), Al(5), and Al(13) and the rest of the atoms are enclosed by the upper island. At an iso-value of 0.88, the upper island first bifurcates at the locations of Al(5) and Al(6). Then the lower ELF iso-surface bifurcates at an iso-value 0.93 at the location of Al(1). The next bifurcation occurs for the upper ELF iso-surface at an iso-value of 0.95 over position of the topmost atom Al(9). At this iso-level, there are three triangular delocalized regions coinciding with rings R6, R6* and on Al(4), Al(5), and Al(13) at the lower tip of CI. It is to be noted that these are the regions of highest aromaticity for the CI cluster. So the aromaticity of CI has a substantial π-electron contribution. Even at an iso-value of 0.99, electrons are delocalized over the bonds connecting Al(7)-Al(2) and Al(3)-Al(11).

The ELF_{σ} at different iso-values have been depicted in Fig. S2. At the 0.70 level, there are three σ-delocalized bands. The central band is located at the center of the triangular core and two other bands are located respectively over three lower Al atoms of the cluster and three upper Al atoms of the cluster. The σ-delocalization is quite strong over the three top Al atoms, as it remains contiguous even at an isovalue of 0.93.

It can be concluded that for the CI cluster, both σ and π aromaticity play an important role. Whereas the central core region is σ-aromatic only, the periphery, top, and bottom of the cluster are both σ and π aromatic.

AIM critical points analysis

According to atoms in molecule (AIM) theory, the nature of covalent bonds can be revealed through topological analysis of the electron density [36]. Bond critical points (BCP) and bond paths for both the Al_{13}^{+} clusters are depicted in Fig. 8. Bond paths are the line of maximum electron density. Nuclear critical points (NCPs) have been represented as violet spheres, bond critical points (BCPs) as orange spheres, and ring critical points (RCPs) as yellow spheres.

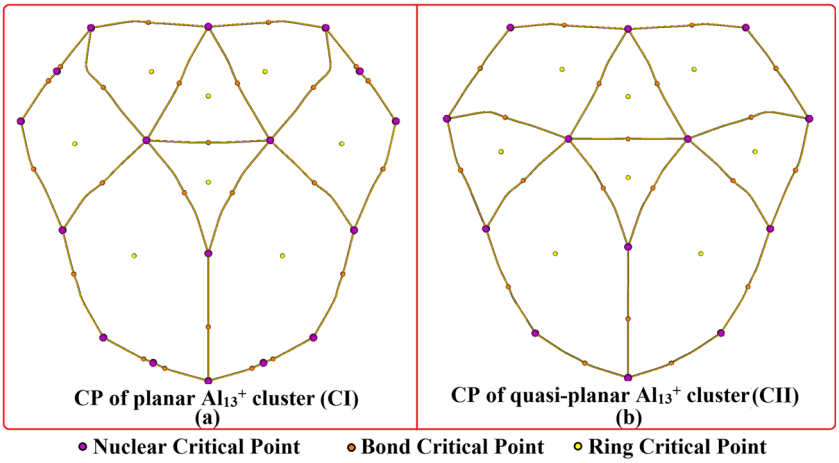

Fig. 8 Critical points of CI and CII cluster through AIM analysis

For the planar CI cluster (Fig. 8a), there are a total of 49 critical points, which satisfies the Poincaré–Hopf relationship. Among these, 17 are NCPs, 24 are BCPs, and 8 are RCPs. It is interesting to note that although the geometrical configuration of the cluster contains 14 rings and 24 inter-aluminium bonds (Fig. 1a), the AIM analysis shows only eight rings formed by the bond paths. Each ring has a single ring critical point at the center. The number of NCP for the present cluster exceeds the number of nucleus present in the cluster. Bond critical points are arranged in five parallel sets. The topmost row consists of two BCPs, the second row consists of eight BCPs, the third row consists of six BCPs, the fourth row consists of three BCPs, and the lowermost fifth row consists of four BCPs. There is also a BCP in between the NCPs corresponding to Al(2) and Al(3).

For the quasi-planar Al_{13}^+ cluster, there are a total of 41 critical points satisfying the Poincaré–Hopf relationship (Fig. 8b). Among these, 13 are NCPs, 20 are BCPs, and 8 are RCPs. For this cluster, the RCPs are also located at the center of eight rings formed by the bond paths. The number of NCPs in this cluster is equal to the number of nucleus present in the cluster. Here, bond critical points are arranged in six parallel sets. The topmost row consists of two BCPs, the second row consists of four BCPs, the third row consists of three BCPs, the fourth row consists of six BCPs, the fifth row has three BCPs, and the sixth row has two critical points. The distribution of the critical points also maintains the bilateral symmetry of the cluster.

In terms of this topological analysis, it can be concluded that although the lower half of both CI and CII are identical in a topological sense, the upper portion of CI has a unique topological difference with that of CII.

AdNDP analysis

Adaptive natural density partitioning (AdNDP) is a tool for gaining insight into the nature of electron distribution and sharing among the individual atoms forming the cluster. It is a multicenter bonding analysis tool that reveals how electron pairs are distributed over multiple atom centers. The result of AdNDP analysis for the planar Al_{13}^+ cluster (CI) is depicted in Fig. 9a, which reveals that besides 2c-2e bonds, the cluster possess 3c-2e, 4c-2e, and 5c-2e bonds. Ten 2c-2e bonds exist among the ten peripheral Al atoms. The electron occupancies of these bonds range from 1.8892 to 1.9456. The contiguous nature of these bonds indicates a σ-bonded framework for the ten peripheral Al atoms of the cluster. There are six 3c-2e σ-bonds. Among these, the one with the highest occupancy (ON = 1.9179) is delocalized over the three central Al atoms forming the core of the cluster. Five other 3c-2e σ-bonds act as bridges between the peripheral ring and the central core with occupancies ranging 1.7734 to 1.8042. The 4c-2e π-bond with occupancy 1.6498 is spread over four Al atoms [Al(1), Al(4), Al(5), Al(13)] forming the lower tip of the cluster. There are two 5c-2e π-bonds (ON = 1.7320) substantially spread over the left half and right half of the cluster. Thus, the present Al_{13}^+ cluster has a double aromatic character; it is both π and σ aromatic.

The result of AdNDP analysis for the quasi-planar Al_{13}^+ cluster (CII) is depicted in Fig. 9b, which reveals that this cluster contains ten 2c-2e bonds, six 3c-2e bonds, one 4c-2e bond, and two 5c-2e bonds. Even though the present cluster is not perfectly planar, the ten 2c-2e bonds still exist among ten peripheral Al atoms. The electron occupancies of these bonds range from 1.8828 to 1.9330. The contiguous nature of these bonds indicates a σ-bonded framework. It is to be noted that the occupancy number of each of the peripheral 2c-2e σ-bonds for CII is lower than the corresponding bonds of CI. This nicely correlates with the enhanced peripheral bond lengths of the quasi-planar CII cluster compared to the planar CI cluster. Like CI, in CII there also exist six 3c-2e σ-bonds. Among these, the bond with highest occupancy (ON = 1.9245) is delocalized over the three central Al atoms. Five other 3c-2e σ-bonds act as bridges between peripheral ring and the central core with occupancy ranging from 1.7776 to

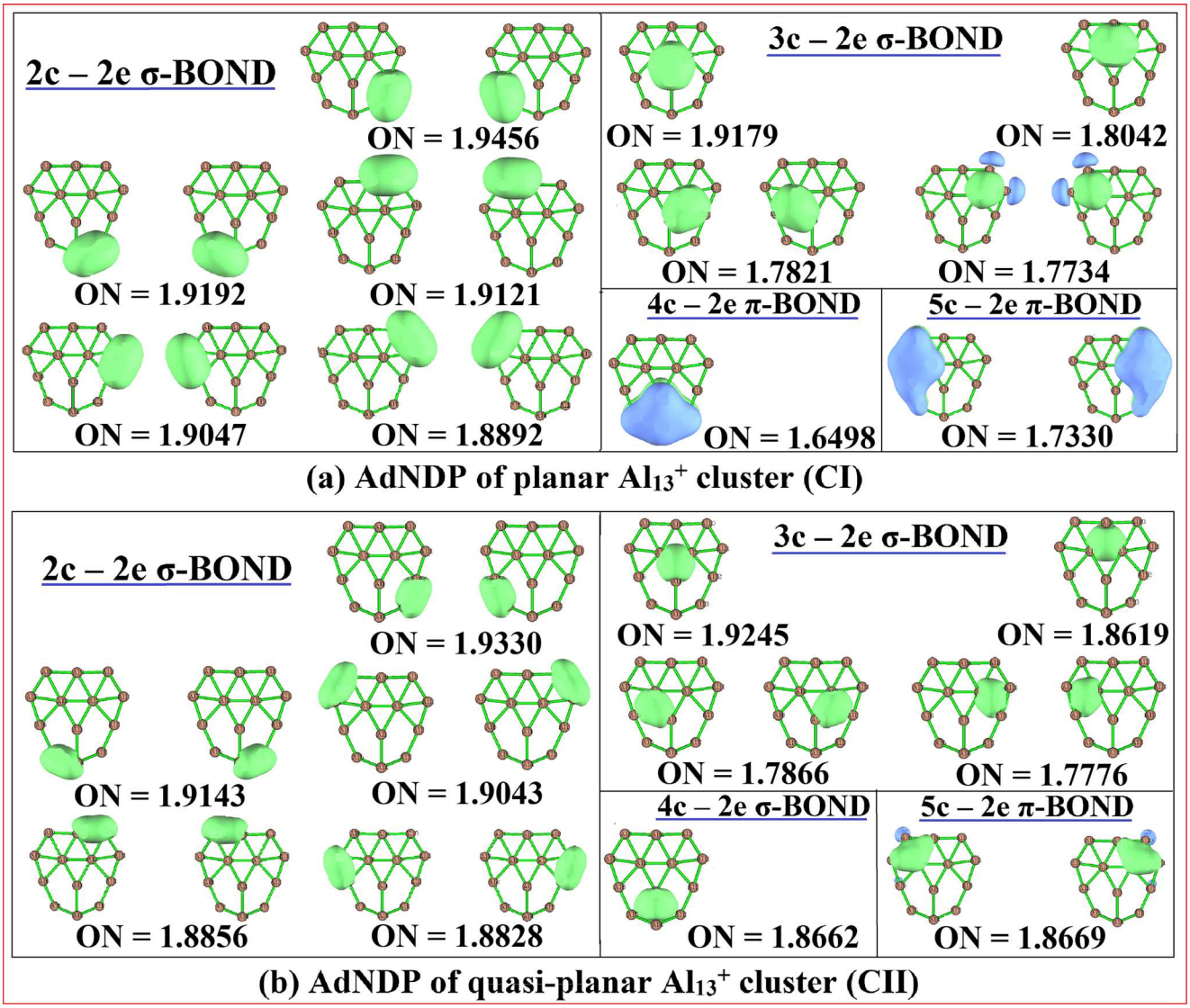

Fig. 9 Adaptive natural density partitioning (AdNDP) analysis of planar and quasi-planar Al_{13}^+ cluster

1.8619. The occupancy number of each of the six 3c-2e of CII is higher than that of CI. This indicates that more electrons reside in and around the core in the CII cluster compared to CI. In sharp contrast to CI, the 4c-2e bond in CII is a σ-bond instead of a π-bond. The occupancy of this 4c-2e σ-bond is 1.8662, which is substantially higher than that of 4c-2e π-bond of CI (ON = 1.6498). This bond is spread over four Al atoms [Al(1), Al(4), Al(5), Al(13)], forming the lower tip of the cluster. There are also two 5c-2e π-bonds in CII with occupancy 1.8669, but these bonds have a mixed π-σ character. Unlike the CI cluster, these bonds are now more localized over the upper left corner and upper right corner of the cluster. Thus, the quasi-planarity of the present Al_{13}^+ cluster can be assigned to the non-existence of π-delocalization. By comparing the AdNDP analysis of both the clusters, it can be concluded that the quasi-planar CII cluster has achieved more stability due to transformation of π-electrons into σ-electrons. Thus, the aromatic nature of the quasi-planar CII cluster is more of σ-character, but that of the planar CI cluster is a combination of both π and σ character.

Recently, two interesting boron clusters, B_{13}^+ and B_{19}^-, have been reported, which possess planar geometry, and their planarity has been assigned to the aromatic character of the respective clusters [37]. With aluminium being located in the same group as boron, it is worth comparing the nature of bonding of the Al_{13}^+ clusters with that of the B_{13}^+ cluster. Whereas B_{13}^+ is globally aromatic, the Al_{13}^+ clusters reported here are quite different in nature—they have antiaromatic domains within a global aromatic sea.

Conclusions

In summary, for the first time, we have found two closely related Al_{13}^+ clusters—one perfectly planar and the other quasi-planar. The quasi-planar structure is a lower-energy structure than the planar structure. These clusters have a bilateral symmetry. Both the clusters have an isosceles triangular core that is encircled by a ring of ten Al atoms. The transition from planarity to quasi-planarity results from the substantial charge transfer from the periphery to the core of the cluster and subsequent redistribution over different atoms leading to enhancement and reversal of dipole moment direction. NICS study reveals that both the clusters are globally aromatic with localized antiaromatic regions embedded within an aromatic sea. Antiaromatic regions are characterized by enhanced bond lengths among the atoms located in these regions. The enhanced stability of the quasi-planar structure correlates well with the improved global aromatic character of it compared to the planar structure. AdNDP analysis reveals that the planar cluster is both σ and π-aromatic but the quasi-planar structure is mostly σ-aromatic. The enhanced aromatic character of the quasi-planar structure can be correlated with the transfer of π-delocalized electrons into the σ-delocalized framework of this cluster. This conclusion is again corroborated by the ELF study, which reveals that for the quasi-planar structure, the total ELF iso-surface is more delocalized over the periphery than that of the planar cluster. In the conversion of the planar structure to the quasi-planar structure, the peripheral rings are drastically affected by going out of plane with respect to the core of the cluster. In this rearrangement, the π-electrons of the peripheral ring transform to σ-delocalized electrons. Thus, the electronic structural analysis of two closely related Al_{13}^+ clusters have provided deeper insight into the nature of the charges redistribution, consequent structural rearrangement and the effect of this on aromaticity of the clusters. The present Al_{13}^+ clusters are not only rare examples of systems having coexistence of aromatic and antiaromatic regions side by side but also the study of these systems reveals that even a non-planar structure can sometimes have greater aromaticity compared to its planar counterpart.

Acknowledgements Atish Dipankar Jana acknowledges financial support from the Department of Science, Technology and Biotechnology, Government of West Bengal, India, through the project no ST/P/S&T/16G-47/2017.

References

1. Purath A, Köppe R, Schnöckel H (1999) An $Al_{12}R_8^-$ cluster as an intermediate on the way from aluminium(I) compounds to aluminium metal. Chem Commun 1933–1934. https://doi.org/10.1039/A904247D
2. Lloyd LD, Johnston RL (1998) Modelling aluminium clusters with an empirical many-body potential. Chem Phys 236:107–121. https://doi.org/10.1016/S0301-0104(98)00180-3
3. Liu ZY, Wang CR, Huang RB, Zheng LS (1995) Mass Distributions of Binary Aluminum Cluster Anions $Al_nX_m^-$ (X=O, S, P, As, C). Int J Mass Spectrom Ion Process 141:201–208. https://doi.org/10.1016/0168-1176(95)04103-R
4. Zhen HL, Jasper AW, Truhlar DG (2007) Structures, rugged energetic landscapes, and nanothermodynamics of Aln ($2 \leq n \leq 65$) particles. J Am Chem Soc 129:14899–14910. https://doi.org/10.1021/ja073129i
5. Walsh N, Martinez F, Marx G, Schweikhard L, Ziegler F (2009) Multiply negatively charged aluminium clusters II. Production of Al_n^{3-}. Eur Phys J D 52:27–30. https://doi.org/10.1140/epjd/e2008-00255-3
6. Hass KC, Schneider WF, Curioni A, Andreoni W (1998) The chemistry of water on alumina surfaces: reaction dynamics from first principles. Science 282(80):265–268. https://doi.org/10.1126/science.282.5387.265
7. Jayaraman K, Chakravarthy SR, Sarathi R (2011) Quench collection of nano-aluminium agglomerates from combustion of sandwiches and propellants. Proc Combust Inst 33:1941–1947. https://doi.org/10.1016/j.proci.2010.06.047
8. Liu Y, Hua Y, Jiang M, Jiang G, Chen J (2012) Theoretical study of the geometries and dissociation energies of molecular water on neutral aluminum clusters Aln(n = 2-25). J Chem Phys 136:0–9 . https://doi.org/10.1063/1.3685603
9. Maatallah M, Guo M, Cherqaoui D, Jarid A, Liebman JF (2013) Aluminium clusters for molecular hydrogen storage and the corresponding alanes as fuel alternatives: a structural and energetic analysis. Int J Hydrog Energy 38:5758–5767. https://doi.org/10.1016/j.ijhydene.2013.03.015
10. Bergeron DE, Roach PJ, Castleman AW, Jones NO, Khanna SN (2005) Al cluster superatoms as halogens in polyhalides and as alkaline earths in iodide salts. Science 307(80):231–235. https://doi.org/10.1126/science.1105820
11. Cox DM, Trevor DJ, Whetten RL, Rohlfing EA, Kaldor A (1986) Aluminum clusters: magnetic properties. J Chem Phys 84:4651–4656. https://doi.org/10.1063/1.449991
12. Rao BK, Jena P (1999) Evolution of the electronic structure and properties of neutral and charged aluminum clusters: a comprehensive analysis. J Chem Phys 111:1890–1904. https://doi.org/10.1063/1.479458
13. Lloyd LD, Johnston RL, Roberts C, Mortimer-Jones TV (2002) Geometry optimisation of aluminium clusters using a genetic algorithm. ChemPhysChem 3:408–415. https://doi.org/10.1002/1439-7641(20020517)3:5<408::AID-CPHC408>3.0.CO;2-G
14. Ouyang Y, Wang P, Xiang P, Chen H, Du Y (2012) Density-functional theory study of Al_n and $Al_{n-1}Mg$ (n=2-17) clusters. Comput Theor Chem 984:68–75. https://doi.org/10.1016/j.comptc.2012.01.012
15. Jones RO (1993) Simulated annealing study of neutral and charged clusters: Al_n and Ga_n. J Chem Phys 99:1194–1206. https://doi.org/10.1063/1.465363
16. Wright JS (1974) Stability and aromaticity of nitrogen rings. N_3^+, N_4, and N_6. J Am Chem Soc 96:4753–4760. https://doi.org/10.1021/ja00822a005
17. Havenith RWA, Jiao H, Jenneskens LW, Lenthe JHv, Sarobe M, Schleyer PvR, Kataoka M, Necula A, Scott LT (2002) Stability and aromaticity of the cyclopenta-fused pyrene congeners. J Am Chem Soc 124:2363–2370. https://doi.org/10.1021/ja011538n
18. Matxain JM, Ugalde JM, Towler MD, Needs RJ (2003) Stability and aromaticity of B_iN_i rings and fullerenes. J Phys Chem A 107:10004–10010. https://doi.org/10.1021/jp036296n

19. Martín-Santamaría S, Rzepa HS (2000) Double aromaticity and anti-aromaticity in small carbon rings. Chem Commun:1503–1504. https://doi.org/10.1039/b002922j
20. Chen Z, Wannere CS, Corminboeuf C, Puchta R, Schleyer PvR (2005) Nucleus-independent chemical shifts (NICS) as an aromaticity criterion. Chem. Rev. 105:3842–3888. https://doi.org/10.1021/cr030088+
21. Portella G, Poater J, Solà M (2005) Assessment of Clar's aromatic π-sextet rule by means of PDI, NICS and HOMA indicators of local aromaticity. J. Phys. Org. Chem. 18:785–791. https://doi.org/10.1002/poc.938
22. Fallah-Bagher-Shaidaei H, Wannere CS, Corminboeuf C, Puchta R, Schleyer PvR (2006) Which NICS aromaticity index for planar π rings is best? Org Lett 8:863–866. https://doi.org/10.1021/ol0529546
23. Galeev TR, Chen Q, Guo J-C, Bai H, Miao C-Q, Lu H-G, Sergeeva P, Li S-D, Boldyrev AI (2011) Deciphering the mystery of hexagon holes in an all-boron graphene α-sheet. Phys Chem Chem Phys 13:11575. https://doi.org/10.1039/c1cp20439d
24. Moreno D, Pan S, Zeonjuk LL, Islas R, Osorio E, Martinez-Guajardo G, Chattaraj PK, Heine T, Merino G (2014) B_{18}^{2-} : a quasi-planar bowl member of the Wankel motor family. Chem Commun 50:8140–8143. https://doi.org/10.1039/C4CC02225D
25. Kumar A, Duran M, Solà M (2017) Is coronene better described by Clar's aromatic π-sextet model or by the AdNDP representation? J Comput Chem 38:1606–1611. https://doi.org/10.1002/jcc.24801
26. Poater J, Duran M, Sola M, Silvi B (2005) Theoretical evaluation of Electron delocalization in aromatic molecules by means of atoms in molecules (AIM) and electron localization function (ELF) topological approaches. Chem Rev 105:3911. https://doi.org/10.1021/cr030085x
27. Bader RFW, Matta CF (2004) Atomic charges are measurable quantum expectation values: a rebuttal of criticisms of QTAIM charges. J Phys Chem A 108:8385–8394. https://doi.org/10.1021/jp0482666
28. Salasco L, Dovesi R, Orlando R, Causa M, Saunders VR (1991) A periodic ab initio extended basis set study of α-Al_2O_3. Mol Phys 72:267–277. https://doi.org/10.1080/00268979100100201
29. Frisch MJ, Trucks GW, Schlegel HB, Scuseria GE, Robb MA, Cheeseman JR, Montgomery JJA, Vreven T, Kudin KN, Burant JC, Millam JM, Iyengar SS, Tomasi J, Barone V, Mennucci B, Cossi M, Scalmani G, Rega N, Petersson GA, Nakatsuji H, Hada M, Ehara M, Toyota K, Fukuda R, Hasegawa J, Ishida M, Nakajima T, Honda Y, Kitao O, Nakai H, Klene M, Li X, Knox JE, Hratchian HP, Cross JB, Adamo C, Jaramillo J, Gomperts R, Stratmann RE, Yazyev O, Austin AJ, Cammi R, Pomelli C, Ochterski JW, Ayala PY, Morokuma K, Voth GA, Salvador P, Dannenberg JJ, Zakrzewski VG, Dapprich S, Daniels AD, Strain MC, Farkas O, Malick DK, Rabuck AD, Raghavachari K, Foresman JB, Ortiz JV, Cui Q, Baboul AG, Clifford S, Cioslowski J, Stefanov BB, Liu G, Liashenko A, Piskorz P, Komaromi I, Martin RL, Fox DJ, Keith T, Al-Laham MA, Peng CY, Nanayakkara A, Challacomb M, Gill PMW, Johnson B, Chen W, Wong MW, Gonzalez C, Pople JA (2004) Gaussian 03, revision C.02. Gaussian, Inc, Wallingford CT
30. Lu T, Chen F (2012) Multiwfn: a multifunctional Wavefunction Analyser. J Comp Chem 33:580–592. https://doi.org/10.1002/jcc.22885
31. Portman S, Lüthi PH (2000) MOLKEL: an interactive molecular graphics tool. CHIMIA 54:763
32. Skripnikov L (2012) Chemissian, a computer program to analyse and visualise quantum-chemical calculations. www.chemissian.com
33. Becke AD, Edgecombe KE (1990) A simple measure of electron localization in atomic and molecular system. J Chem Phys 92:5397–5403. https://doi.org/10.1063/1.458517
34. Bader RFW, Heard GL (1999) ELF lone pairs and covalent bonds. J Chem Phys 111:878935
35. Silvi B (2002) The synaptice order: a key concept to understand multicenter bonding. J Mol Struct 614:3–10. https://doi.org/10.1016/S0022-2860(02)00231-4
36. Bader RFW (1990) Atoms in molecules: Wiley Online Library
37. Martínez-Guajardo G, Sergeeva AP, Boldyrev AI, Heine T, Ugalde JM, Merino G (2011) Unravelling phenomenon of internal rotation in B_{13}^+ through chemical bonding analysis. Chem Commun 47:6242–6244. https://doi.org/10.1039/c1cc10821b